Ultra-thin 3D Nano-Devices from Atomic Layer Deposition on Polyimide

*Nathan T. Eigenfeld, Jason M. Gray, Joseph J. Brown, George D. Skidmore, Steven M. George, and Victor M. Bright**

Efforts to improve upon current nano and micro electro-mechanical systems (N/MEMS) with continually shrinking dimensions and increased performance require new processing and fabrication techniques. Recently, bottom-up and top-down fabrication methods have shown unique advancements in applications of nanoscale polymeric structures in hierarchical arrangements.[1] However, fabrication methods which incorporate both inorganic and organic materials will offer a more versatile platform for N/MEMS fabrication and nanotechnology advancement. This paper demonstrates a repeatable and extendable top-down fabrication method combining standard lithography and etching techniques with atomic layer deposition (ALD) generated ultra-thin films on polyimide substrates with three-dimensional features. This fabrication method was demonstrated in a variety of ALD materials including Al_2O_3, W and Ru with thicknesses on the order of 10 nm and in a variety of two-dimensional patterns that included two-story suspended structures. Three-dimensional structural property control was achieved with three-dimensional molds that increased cantilever beam rigidity. Residual curl of cantilevers was observed in cantilevers of varied thicknesses and compared to a continuum model. Finally, an absorption structure for a microbolometer infrared light sensing pixel was fabricated and tuned for flatness using nanometer-scale thickness control enabled by ALD.

Traditional bulk and surface micromachining techniques have provided a robust and diverse platform for the fabrication of microelectronics and micromachines or sensors.[2,3] Polymer applications in microfabrication processes are a subset of a growing trend of electrically, thermally, mechanically, and optically active organic material systems for flexible and stretchable electronics, organic light emitting diodes, and nano and micro electro-mechanical systems (N/MEMS) fabrication.[4–7] Spin-coated polymers such as polyimide or polydimethylsiloxane are easily moldable or made into flexible layers for micro-sensing devices or micro-fluidic channels.[5,8–10] Furthermore, dry etching of sacrificial polymers is very advantageous over traditional wet release of microdevices in Si based microscale and nanoscale fabrication. The use of dry etching to release suspended structures at these scales avoids stiction and supercritical CO_2 processing.[11]

New nanotechnologies will require high performance and reliable inorganic and organic material interfacing to excel beyond traditional fabrication methods. Such a task is challenging due to the chemical and temperature sensitivity of many organic materials. High temperatures from chemical vapor deposition can cause a glass transition or thermal breakdown, while harsh conditions from plasma-assisted vapor deposition or sputtering can cause pinholes or degradation in the polymer. Additionally, many current deposition techniques face limitations in thickness control and film conformality and continuity at the nanoscale. ALD is an increasingly popular thin film deposition method which uses a self-limiting binary reaction sequence that deposits films in discrete steps limited by surface site chemical reactions.[12–14] It typically produces continuous pinhole-free films with atomically controlled thicknesses, high conformality, and atomically smooth surfaces. These are essential properties as design constraints push device technologies to ever smaller sizes.[15,16] ALD-generated films on traditional microfabrication substrates have recently been applied to N/MEMS applications.[17–23]

Because ALD may be performed at low deposition temperatures and without high energy ion bombardment, fabrication by ALD on polymers avoids problems associated with other deposition techniques on polymers and thereby may enable a new generation of devices. Inorganic ALD material generation on organic polymers has been found to be a reliable, scalable, and high-performing method utilizing aluminum oxide (Al_2O_3) as a model material.[24,25] Other materials are available in conformal ALD because Al_2O_3 is often used as a seed layer for the growth of metal, semiconducting and insulating layers including, but not limited to W, Ru, Pt, ZnO, TiO_2 and SiO_2.[13,14,26–29] Polymers may also be used as insulating layers, adhesion layers, thermal barrier layers, encapsulating biocompatible gels, moldable substrates, and flexible or stretchable substrates. ALD materials have uses as electrical, mechanical, or optical layers for patterned N/MEMS, and may offer many advantageous coatings for gas diffusion applications and microsystem packaging.[30–32]

As shown in **Figure 1**, ALD of laminate films was performed on a polyimide mold with vias, trenches and exposed electrical interconnect layers. This laminate was demonstrated

N. T. Eigenfeld, Dr. J. M. Gray, Dr. J. J. Brown, Prof. V. M. Bright
Department of Mechanical Engineering
University of Colorado at Boulder
1111 Engineering Drive, 427 UCB,
Boulder, CO 80309–0427, USA
E-mail: victor.bright@colorado.edu

Prof. S. M. George
Department of Chemistry and Biochemistry
and Department of Mechanical Engineering
University of Colorado at Boulder, 215 UCB,
Boulder, CO 80309–0215, USA

Dr. G. D. Skidmore
Network and Imaging Systems DRS ITS Texas Site
13532 North Central Expwy SC Bldg,
Dallas, TX 75243, USA

DOI: 10.1002/adma.201400410

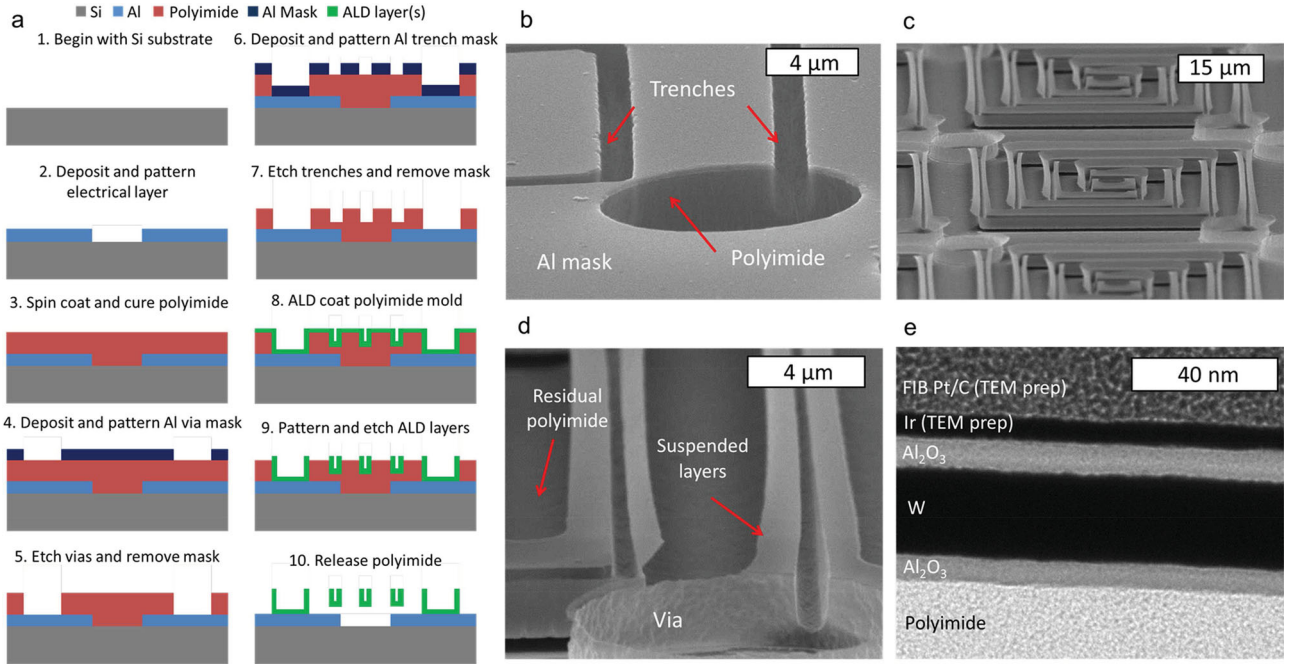

Figure 1. Fabrication processing overview. a) Fabrication process steps 1–10 with descriptions. The process may be extended to multiple levels by repeating steps 3–9 before finishing with release step 10. b) Etched polyimide mold of vias and trenches with aluminum mask. The via is nominally 3 µm deep and open to the underlying metal layer and connected to a 1.5 µm deep trench pattern. c) Partially released structures consisting of 2.2 nm Al_2O_3/18 nm W/2.2 nm Al_2O_3. The ALD layers coat the via and trench mold from (b). d) Magnified view of a portion of the structures in (c). e) TEM cross-sectional image of an Al_2O_3/W/Al_2O_3 coating on polyimide with similar thicknesses to (c) and (d). All images in (b-d) were taken with an SEM at a 75° stage tilt angle.

experimentally from a metal layer of W or Ru surrounded by two ALD Al_2O_3 layers. The bottom layer coated the polyimide and promoted nucleation of the metal layer, and the top layer protected against oxidation of the metal layer and/or balanced stress gradients to promote flatness in the final structure.[13,25] Although Al_2O_3 was present between the ALD metal and the electrode, it was sufficiently thin that electrical connection was readily achieved through the Al_2O_3. With an extended fabrication process (Figure 1a), two-level suspended structures with a 13.5 nm thickness laminate of Al_2O_3/Ru/Al_2O_3 were fabricated, shown in **Figure 2**a. By utilizing polymer sacrificial layers over traditional SiO_2 layers, smooth additive processing levels are easily spun on at thicknesses ranging from tens of nm to hundreds of µm. Additional device levels are built by spinning on additional polyimide layers over existing ALD patterns on underlying polyimide, a task not easily accomplish by traditional Si micro-machining. These additional polyimide levels may be selectively processed without damaging the underlying ALD layers. The process is likely to be extendable to any number of levels as long as the final structure is designed to be mechanically robust and self-supporting. These ALD laminates produce very robust structures. For example, in Figure 2a, the first level fixed-fixed cantilevers have length to thickness aspect ratios of 10^4 and remain very flat, even while supporting multiple anchors from second level cantilevers.

By utilizing standard lithography methods in this process, batch fabrication of any pattern that can be achieved with micro or nanolithography is possible. A variety of patterns with suspended ALD laminates with W and Ru surrounded by Al_2O_3 may be seen in Figure 2. Figure 2b demonstrates an array of Al_2O_3/W/Al_2O_3 structures curled upwards, potentially useful for engineered 3-D metamaterials.[9,33,34] Figure 2c and Figure 2e demonstrate flower petal patterns for potential applications such as nano-trapping systems for single cell biological testing platforms.[35,36] Flat structures are also achievable through stress balancing or additional mechanical reinforcement (Figure 2d and Figure 2f).

N/MEMS devices continually face mechanical issues surrounding residual stress effects from both intrinsic film stress and fabrication conditions. To suspend flat or specifically curled structures, control over the properties of these active thin films is vital. Motivated by prior work with polysilicon ALD coated trench molds, control of mechanical properties by incorporating a three-dimensional mold in the sacrificial polyimide layer was demonstrated.[22,23] **Figure 3** demonstrates the effect of a trench in structural reinforcement of fixed-free cantilevers. Without the trench (Figure 3a), the large bi-axial stress curls the cantilevers. With the addition of the trench in the cross section (Figure 3b), the device stiffness was substantially increased. For a flat beam with thickness t, width b, and effective Young's modulus E_{eff}, the flexural rigidity EI about the x–axis is given as,[37]

$$EI_{flat} = E_{eff} bt^3/12. \quad (1)$$

For a channel section with depth z and width d (Figure 3c), the y–axis centroid coordinate C_y, channel area A, and flexural rigidity about the x–axis of the full trench structure from the bottom of Figure 3c EI_{trench}, are given as,[37]

Adv. Mater. 2014,
DOI: 10.1002/adma.201400410

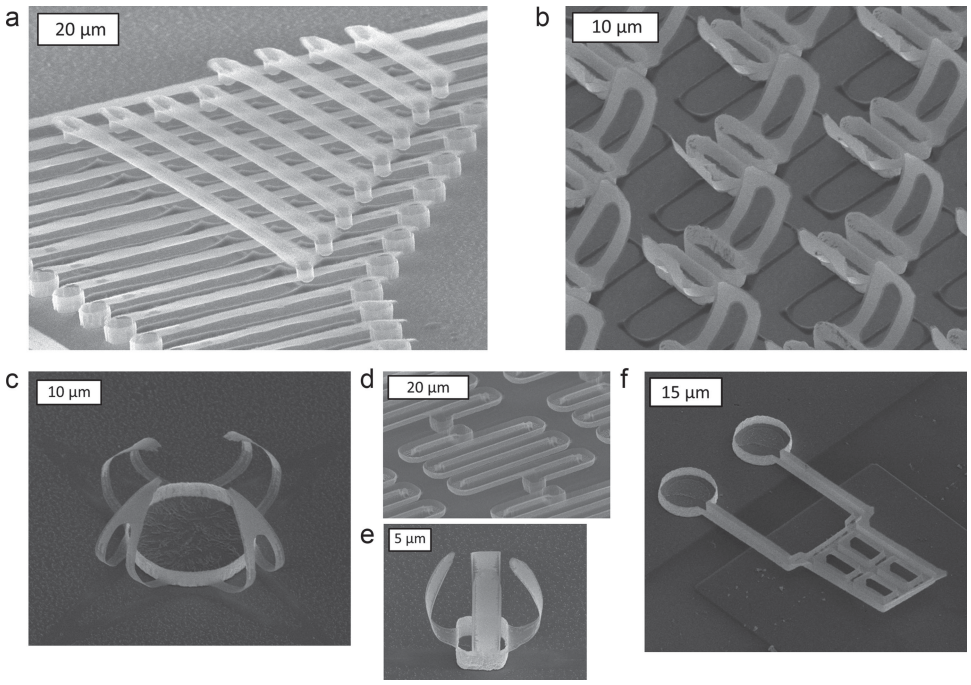

Figure 2. SEM images of a variety of fully released microstructures fabricated using the process from Figure 1a. a) Two-story suspended fixed-fixed cantilever structures comprised of 5.5 nm Al_2O_3/2.5 nm Ru/5.5 nm Al_2O_3 fabricated from the extended process outlined in Figure 1a. The second level vias are etched to the underlying first level patterned nanostructures and the deposition and patterning repeated. A short lithography step at step 5 of the extended process of Figure 1a is incorporated to fill the vias and protect the 1st level ALD from being etched during the Al mask removal. b) Array of meta-material-like structures comprised of 5.5 nm Al_2O_3/18 nm W/5.5 nm Al_2O_3. c) Curled structures comprised of 5.5 nm Al_2O_3/5 nm Ru/7.7 nm Al_2O_3. d) Microbolometer-like structure with trench, comprised of 5.5 nm Al_2O_3/5 nm Ru/7.7 nm Al_2O_3. e) Curled structure comprised of 5.5 nm Al_2O_3/5 nm Ru/7.7 nm Al_2O_3. f) Micromechanical paddle structure comprised of 2.2 nm Al_2O_3/18 nm W/2.2 nm Al_2O_3. Images (a) and (d) were taken at a 60° stage tilt angle and (b),(d),(e) and (f) at a 45° stage tilt angle.

$$C_y = \frac{2z^2t + (d-2t)t^2}{2zd - 2(d-2t)(z-t)} \tag{2}$$

$$A = 2tz + (d-2t)t \tag{3}$$

$$EI_{trench} = E_{eff}\left[\frac{1}{12}\left(b-(d-2t)\right)t^3 + \frac{1}{3}\left((d-2t)t^3 + 2tz^3\right) - AC_y^2\right] \tag{4}$$

The first term in the brackets of EI_{trench} accounts for the moment of inertia of the flat overhang sections of the trench and the rest for the moment of inertia for the trench. For example, the flexural rigidity of the trench inset beam from Figure 1b for a stress free structure with d = ~1.5 µm and z = ~1.6 µm, is ~10^4 times larger than the flat beam in Figure 1a with the same width, thickness and effective Young's modulus. This trench method may be used to ensure mechanical flatness when other optical, thermal or electrical performance constraints require film thicknesses or material combinations that would produce curled release structures without the trench. Additionally, the trench process may be used to induce targeted physical shapes such as three-dimensional helices as depicted in Figure 3e. Trench insets placed in angled increments along the cantilever structures (Figure 3d) forced the structure to spiral upon release (Figure 3e and Figure 3f).

Figure 4a shows the suspension of laminate fixed-free cantilevers of varying length. Four chips underwent identical ALD growth and processing conditions, but with varied Ru thicknesses from ~1.5 nm – 5 nm and outer Al_2O_3 layers with constant 5.5 nm thicknesses. To reduce anchor influence, the fabrication process from Figure 1a was abbreviated by excluding vias and trenches to release ALD structures anchored directly to polyimide. Cantilever curl magnitudes from suspended arrays on each chip were measured and Figure 4b shows the relation between curl and Ru thickness. With atomically controlled ALD material thicknesses, a desired curl level, i.e., high curl for a self-assembled structure, or no curl for a traditional MEMS device structure, may be obtained by atomically tuning material thicknesses.

Only recently have ALD material mechanics with thicknesses on the order of 50 – 100 nm been investigated for single materials, leaving models for laminate structures at <5 nm thicknesses absent in the literature.[19] Intrinsic stresses such as Volmer-Weber grain growth stress, surface interface stress and grain boundary stress are present in these ALD laminates, which are a combination of amorphous and nano-crystalline structures.[38] To best fit the data in Figure 4b, the stress-based curvature for a trimorph cantilever with identical top and bottom material layers was derived.[39] For this trimorph special case, the curvature is given as the following:

ADVANCED MATERIALS
www.advmat.de

www.MaterialsViews.com

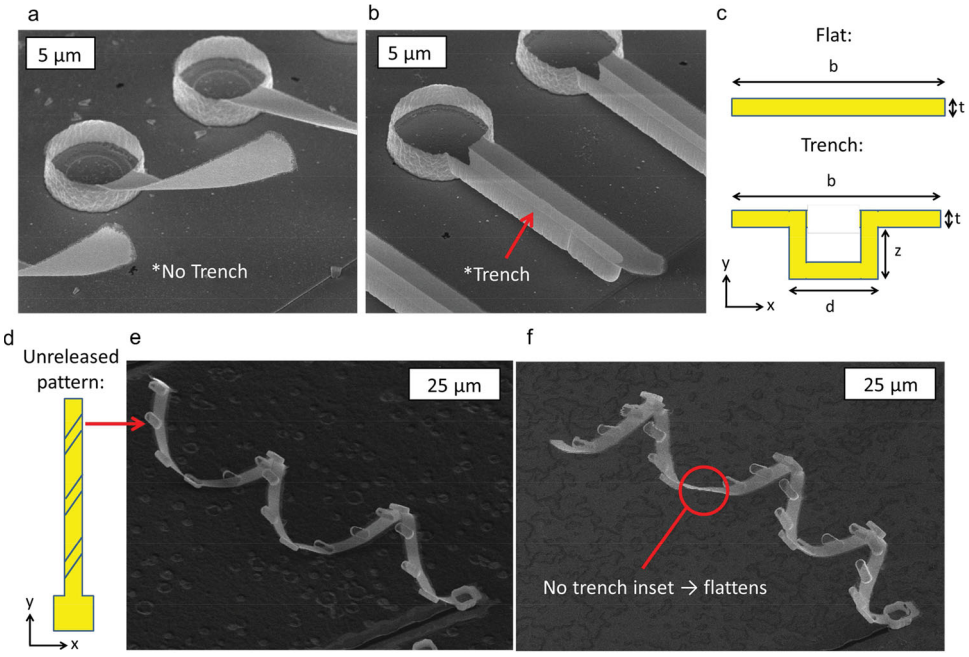

Figure 3. SEM images of freestanding structures that demonstrate the use of patterned trenches for structural control. a) Fixed-free cantilever comprised of 2.2 nm Al_2O_3/18 nm W/2.2 nm Al_2O_3. b) Fixed-free cantilever with same dimensions as (a), but with trench included to maintain mechanical flatness. c) Example of beam cross-sections for flat and trench structures. d) Example of alternative trench layouts for targeted stress relief control in (e) and (f). e) Helical structure comprised of 5.5 nm Al_2O_3/5 nm Ru/7.7 nm Al_2O_3 based off the design from (d). f) Helical structure with missing trench, demonstrating flattening control of cantilever structure where inset is missing. All images were taken at 45° stage tilt angle.

$$\kappa = \frac{6t_3(t_2+t_3)\Delta\sigma_{1-3}}{E_2^2t_2^3 + 2E_3t_3\left(3t_2^2 + 6t_2t_3 + (3+E_3)t_3^2\right)} \quad (5)$$

Here, subscripts denote the layer number of the tri-layer stack counting up from the bottom layer and $\Delta\sigma_{1-3}$ denotes the stress difference between layer 1 and 3. The fitted value for $\Delta\sigma_{1-3}$ is several orders of magnitude larger than expected for standard thin film laminates when fitted with known material thicknesses and material elastic moduli as free parameters capped at bulk values. Because this model lacks detailed consideration of surface stresses associated with nucleation phases of each ALD layer, surface roughness and actual Young's moduli of these ALD films it is not a complete description of the curled cantilever structures described here. Further investigation of ultra-thin film laminate stress specific to ALD generated materials including effects of growth temperature and precursor dosages, is needed for more detailed modeling.

One application for the nanofabrication method described above may be in uncooled microbolometer infrared pixel absorption structures. These devices benefit from extremely low thermal mass, increasing the rate of response to absorbed infrared radiation.[40,41] Commonly, thin resistive metal layers provide optimal absorption properties at thicknesses smaller than 25 nm, but require thick protective dielectric layers sometimes on the order of hundreds of nm. The absorption structures must be extremely flat to ensure maximum absorption and fill-factor in a fabricated array. Using the process outlined in Figure 1a (excluding trenches) an absorption structure comprised of Al_2O_3/W/Al_2O_3 was fabricated with several thicknesses for the top Al_2O_3 layer as shown in Figure 4c-e and a centered mechanical via. The optimal layer thicknesses to produce a flat suspended structure are shown in Figure 4c.

Utilizing the known properties of ALD material formation on polymers in combination with standard MEMS fabrication methods, a new method for top-down N/MEMS manufacturing with three-dimensional features, property control, and atomically controlled curl tuning has been demonstrated. The process is extendable to multiple levels, enabling the possibility of complex hierarchical systems. New opportunities for such devices are enabled by this process wherein the lateral pattern is curled to generate non-planar structures. Further understanding of curl properties is a serious design utility and will no doubt expedite the development of future nanosystems. The multi-level process combined with targeted stress relief could enable complex and even isotropic 3-D meta-material structures.[34] Prior to release, the sample may be coated with biological or chemical particulates to be trapped by flower petal structures upon release and even an electro-mechanical actuation scheme realized. Helical structures from this process target applications such as nano-scale flagella motors for magnetically controlled bio-implantation devices or 3-D helical chiral meta-materials.[34,42,43] This process has also aided in enhancing microbolometer performance by incorporating ultra-thin materials. Further improvements in lithography in combination with the processing defined here will enable suspended nanoscale devices with volumetric footprints on the order of tens of cubic nanometers and may be expected to impact the development of visible frequency meta-materials, optical tuning devices and standard electronics.

DOI: 10.1002/adma.201400410

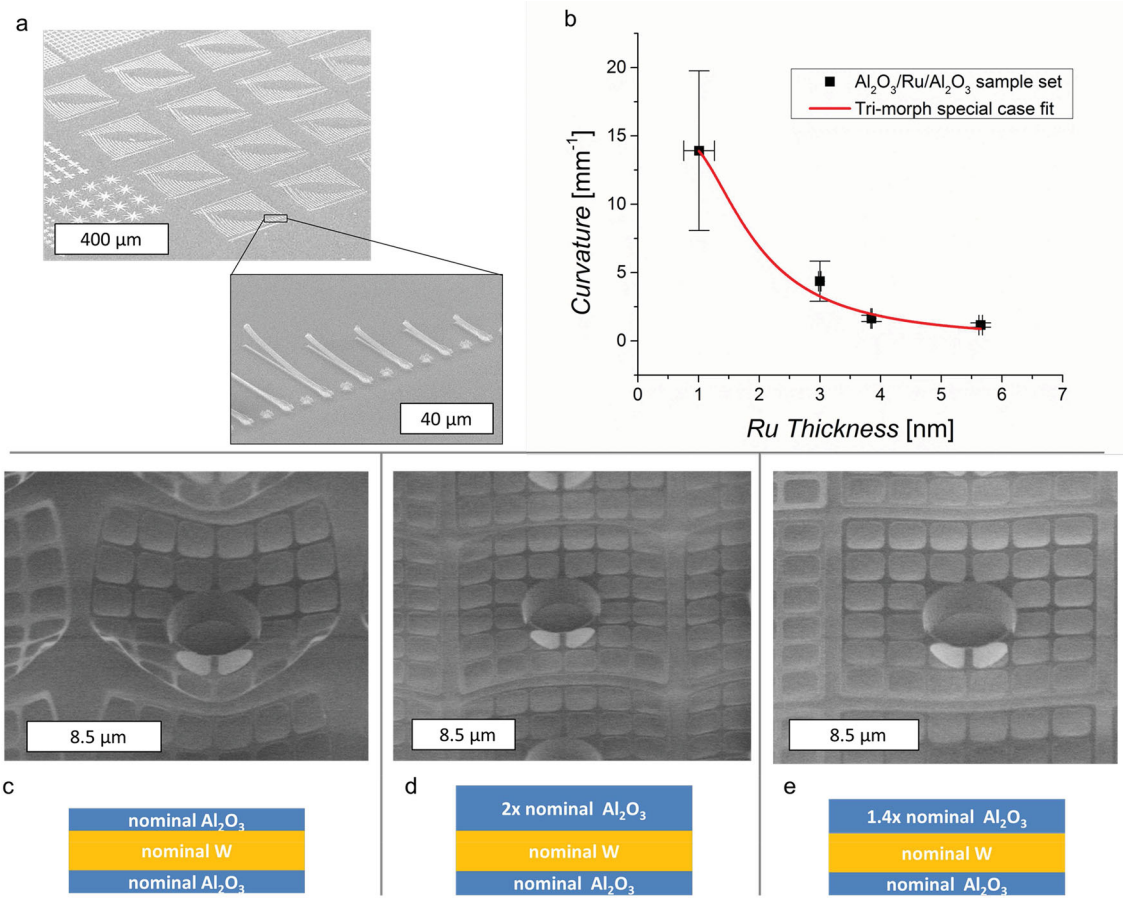

Figure 4. Processing control of curvature. a) Example of suspended $Al_2O_3/Ru/Al_2O_3$ fixed-free cantilever arrays for curl measurements. Inset shows magnified view of curled structures anchored to polyimide. Both SEM images were taken at 60° stage tilt angle. b) Cantilever curvature relates to thickness measured from samples depicted in (a). c-e) SEM images of suspended membranes for microbolometer applications, with cross section of Al_2O_3 (blue) and W (yellow) (not to scale). Only the top Al_2O_3 layer was varied in thickness. Identical W and lower Al_2O_3 layers are used in all three images. Each square structure is 16 µm × 16 µm. c) Nominal top and bottom Al_2O_3 thicknesses resulted in upward curl, while d) a top Al_2O_3 layer two times thicker resulted in downward curl. e) A flat structure was achieved with a 1.4 times nominal top Al_2O_3 layer and nominal bottom Al_2O_3 layer. Images in (c-e) were taken at 45° stage tilt angle.

Experimental Section

Electrical Layer Processing: The electrical layer is formed by evaporation of aluminum and lift-off patterning.

Polyimide Processing: An adhesion promotion chemical, VM-651 is applied to the fabrication substrate and polyimide is spun onto the adhesion layer. The resultant structure was then cured at elevated temperatures. Thicknesses of the structure using this process are typically from about 2.5 µm to about 4.5 µm. Vias and trenches are both etched utilizing a thermally evaporated aluminum mask, which is patterned using negative photoresist and lift-off processing. The polyimide etch is done using anisotropic reactive ion etching (RIE) with O_2 plasma. The aluminum mask is removed in aluminum etchant.

Atomic Layer Deposition: $Al_2O_3/W/Al_2O_3$ ALD is performed at 130 °C in a custom reactor.[13,24] $Al_2O_3/Ru/Al_2O_3$ ALD is performed in a Beneq TFS 200 commercial reactor at 300 °C.[26] The Al_2O_3 uses trimethylaluminum (TMA) and H_2O as gas precursors for growth at ~0.13 nm/cycle. The W uses Si_2H_6 and WF_6 as gas precursors for growth at ~0.384 nm/cycle. Ru uses thermally activated $Ru(EtCp)_2$ and O_2 at 110 °C as gas precursors for growth at ~0.04 nm/cycle. The nucleation of Al_2O_3 forms an initial interfacial layer different from bare Si/SiO_2 substrates possibly due to limited ALD precursor infiltration of the polyimide. In general, this slightly lengthens the nucleation period and results in a skin layer of polyimide/Al_2O_3 which remains unstudied. This skin layer may be discernable in TEM images, but further investigation is required. Growth after nucleation remains highly linear.[25]

Thin Film Micromachining: The ALD lithography is accomplished using a positive photo-resist. Each ALD film is etched by anisotropic RIE using fluorine-based chemistry. The photoresist is removed in an acetone bath.

Release Processing: The patterned ALD is released by removing the polyimide by an isotropic oxygen plasma at 150 W and ~10 Torr in a microdevice asher.

Curl Measurement: Curl was measured with a Zygo white light interferometer by scanning arrays of released cantilevers with a 50 mm working distance objective. Each cantilever's length and deflection was measured with the interferometer's built-in software. Assuming $l << \kappa^{-1}$,[44] curl was calculated from the following:

$$\kappa = 2z / l^2 \tag{6}$$

where z is the vertical deflection and l the length of the cantilever. Statistical and measurement uncertainties were combined and reported with 95% confidence in the intervals shown in Figure 4b.

ALD Thickness Measurement: The deposited ALD film thicknesses were measured from dummy wafers inserted in the reaction chambers during ALD, by use of x-ray reflectometry (XRR) on a Bede D1 x-ray diffractometer (Bede Scientific Ltd.). The x-ray wavelength for measurements was 1.54 Å, corresponding to the *Ka* transition in the Cu x-ray tube. The Bede REFS software was used to fit the XRR data and extract the error in thickness. A Tecnai TEM/STEM with an accelerating voltage of 200 kV was also used for TEM thickness evaluation. TEM sample preparation was carried out using a standard FIB cut out and thinning process.

Acknowledgements

This research was supported by DRS Technologies Inc. and DARPA (Award #W911NF-14-C-007). N.T.E performed most of the writing, process development and data analysis; J.M.G. led initial fabrication development; J.J.B. and V.M.B. conceived, planned, and managed the project, and guided the development and writing processes; and S.M.G. provided expertise in custom ALD reactor development and chemistry. Thanks also to Dr. Layton Baker, Dr. Andrew S. Cavanagh and Jonas C. Gertsch for ALD processing of some of the samples; and Matthias J. Young and Jaclyn K. Sprenger for taking XRR thickness measurements. G.D.S. proposed and provided collaboration to include structures pertinent to microbolometers. Microfabrication and SEM imaging were performed at the Colorado Nanofabrication Laboratory (CNL) and Nanomaterials Characterization Facility (NCF) of the University of Colorado – Boulder. Evans Analytical Group (EAG) performed TEM imaging.

Received: January 25, 2014
Revised: February 20, 2014
Published online:

[1] W.-G. Bae, H. N. Kim, D. Kim, S.-H. Park, H. E. Jeong, K.-Y. Suh, *Adv. Mater.* DOI 10.1002/adma.201303412.
[2] P. J. French, *Sens. Actuators A.* **2002**, *99*, 3.
[3] K. E. Petersen, *Proc. IEEE* **1982**, *70*, 420.
[4] C. Liu, *Adv. Mater.* **2007**, *19*, 3783.
[5] M. Melzer, D. Makarov, A. Calvimontes, D. Karnaushenko, S. Baunack, R. Kaltofen, Y. Mei, O. G. Schmidt, *Nano Lett.* **2011**, *11*, 2522.
[6] J. Meyer, D. Schneidenbach, T. Winkler, S. Hamwi, T. Weimann, P. Hinze, S. Ammermann, H.-H. Johannes, T. Riedl, W. Kowalsky, *Appl. Phys. Lett.* **2009**, *94*, 233305.
[7] K. T. Kamtekar, A. P. Monkman, M. R. Bryce, *Adv. Mater.* **2010**, *22*, 572.
[8] S. A. Dayeh, D. P. Butler, Z. Çelik-Butler, *Sens. Actuators A.* **2005**, *118*, 49.
[9] F. H. Fabreguette, R. A. Wind, S. M. George, *Appl. Phys. Lett.* **2006**, *88*, 013116.
[10] C. Oshman, B. Shi, C. Li, R. Yang, Y. C. Lee, G. P. Peterson, V. M. Bright, *J. Microelectromechanical Syst.* **2011**, *20*, 410.
[11] A. Bagolini, L. Pakula, T. L. M. Scholtes, H. T. M. Pham, P. J. French, P. M. Sarro, *J. Micromech. Microeng.* **2002**, *12*, 385.
[12] S. M. George, *Chem. Rev.* **2010**, *110*, 111.
[13] R. W. Wind, F. H. Fabreguette, Z. A. Sechrist, S. M. George, *J. Appl. Phys.* **2009**, *105*, 074309.
[14] L. Baker, A. S. Cavanagh, D. Seghete, S. M. George, A. J. M. Mackus, W. M. M. Kessels, Z. Y. Liu, F. T. Wagner, *J. Appl. Phys.* **2011**, *109*, 084333.
[15] G. K. Dalapati, Y. Tong, W.-Y. Loh, H. K. Mun, B. J. Cho, *IEEE Trans. Electron Devices* **2007**, *54*, 1831.
[16] M. Knaut, M. Junige, V. Neumann, H. Wojcik, T. Henke, C. Hossbach, A. Hiess, M. Albert, J. W. Bartha, *Microelectron. Eng.* **2013**, *107*, 80.
[17] N. D. Hoivik, J. W. Elam, R. J. Linderman, V. M. Bright, S. M. George, Y. C. Lee, *Sens. Actuators A.* **2003**, *103*, 100.
[18] C. F. Herrmann, F. W. DelRio, D. C. Miller, S. M. George, V. M. Bright, J. L. Ebel, R. E. Strawser, R. Cortez, K. D. Leedy, *Sens. Actuators A.* **2007**, *135*, 262.
[19] M. K. Tripp, C. Stampfer, D. C. Miller, T. Helbling, C. F. Herrmann, C. Hierold, K. Gall, S. M. George, V. M. Bright, *Sens. Actuators A.* **2006**, *130–131*, 419.
[20] Y.-J. Chang, J. M. Gray, A. Imtiaz, D. Seghete, T. Mitch Wallis, S. M. George, P. Kabos, C. T. Rogers, V. M. Bright, *Sens. Actuators A.* **2009**, *154*, 229.
[21] B. D. Davidson, D. Seghete, S. M. George, V. M. Bright, *Sens. Actuators A.* **2011**, *166*, 269.
[22] S. Yoneoka, J. Provine, F. B. Prinz, M. Liger, G. Yama, R. Shuster, F. Purkl, R. T. Howe, T. W. Kenny, *Proc. IEEE MEMS 2011, 24th Int. Conf. Micro Electro Mech. Syst.*, **2011**, 676.
[23] F. Purkl, T. S. English, G. Yama, J. Provine, A. K. Samarao, A. Feyh, B. Kim, G. O'Brien, O. Ambacher, R. T. Howe, *Proc. TRANSDUCERS 2013 Eurosensors XXVII, 17th Conf. Solid-State Sens. Actuators Microsyst.* **2013**, 1507.
[24] C. A. Wilson, J. A. McCormick, A. S. Cavanagh, D. N. Goldstein, A. W. Weimer, S. M. George, *Thin Solid Films* **2008**, *516*, 6175.
[25] C. A. Wilson, R. K. Grubbs, S. M. George, *Chem. Mater.* **2005**, *17*, 5625.
[26] W.-H. Kim, S.-J. Park, D. Y. Kim, H. Kim, *Jounral Korean Phys. Soc.* **2009**, *55*, 32.
[27] J. W. Elam, Z. A. Sechrist, S. M. George, *Thin Solid Films* **2002**, *414*, 43.
[28] J. D. Ferguson, A. R. Yoder, A. W. Weimer, S. M. George, *Appl. Surf. Sci.* **2004**, *226*, 393.
[29] J. W. Klaus, S. M. George, *Surf. Sci.* **2000**, *447*, 81.
[30] P. F. Carcia, R. S. McLean, M. H. Reilly, M. D. Groner, S. M. George, *Appl. Phys. Lett.* **2006**, *89*, 031915.
[31] A. A. Dameron, S. D. Davidson, B. B. Burton, P. F. Carcia, R. S. McLean, S. M. George, *J. Phys. Chem. C* **2008**, *112*, 4573.
[32] M. D. Groner, S. M. George, R. S. McLean, P. F. Carcia, *Appl. Phys. Lett.* **2006**, *88*, 051907.
[33] N. I. Zheludev, *Opt. Photonics News* **2011**, *22*, 30.
[34] C. M. Soukoulis, M. Wegener, *Nat. Photonics* **2011**.
[35] K. Chalapat, N. Chekurov, H. Jiang, J. Li, B. Parviz, G. S. Paraoanu, *Adv. Mater.* **2013**, *25*, 91.
[36] H. Andersson, A. van den Berg, *Curr. Opin. Biotechnol.* **2004**, *15*, 44.
[37] W. Young, R. Budynas, *Roark's Formulas for Stress and Strain*, McGraw-Hill Professional, **2001**.
[38] J. S. Tello, A. F. Bower, *J. Mech. Phys. Solids* **2008**, *56*, 2727.
[39] M. S. Weinberg, *Microelectromechanical Syst. J. Of* **1999**, *8*, 529.
[40] P. W. Kruse, *Uncooled Thermal Imaging: Arrays, Systems, and Applications*, SPIE Press, Bellingham, Wash., USA, **2001**.
[41] C. Li, G. Skidmore, C. Howard, E. Clarke, C. J. Han, (DRS Sensor & Targeting Systems Inc.), *US7,622,717 B2*, **2009**.
[42] L. Zhang, J. J. Abbott, L. Dong, B. E. Kratochvil, D. Bell, B. J. Nelson, *Appl. Phys. Lett.* **2009**, *94*, 064107.
[43] V. Y. Prinz, V. A. Seleznev, A. K. Gutakovsky, A. V. Chehovskiy, V. V. Preobrazhenskii, M. A. Putyato, T. A. Gavrilova, *Phys. E Low-Dimens. Syst. Nanostructures* **2000**, *6*, 828.
[44] W.-H. Chu, M. Mehregany, R. L. Mullen, *J. Micromech. Microeng.* **1993**, *3*, 4.